Angiopoietin 2 mediates microvascular and hemodynamic alterations in sepsis

Tilman Ziegler,[1] Jan Horstkotte,[1] Claudia Schwab,[2] Vanessa Pfetsch,[1] Karolina Weinmann,[1] Steffen Dietzel,[3] Ina Rohwedder,[4] Rabea Hinkel,[1,5] Lisa Gross,[1] Seungmin Lee,[1] Junhao Hu,[6] Oliver Soehnlein,[5,7] Wolfgang M. Franz,[1,5] Markus Sperandio,[3] Ulrich Pohl,[3,5] Markus Thomas,[8] Christian Weber,[5,7] Hellmut G. Augustin,[6] Reinhard Fässler,[4,5] Urban Deutsch,[2] and Christian Kupatt[1,5]

[1]Medizinische Klinik und Poliklinik I, Klinikum Großhadern, Ludwig Maximilians University, Munich, Germany. [2]Theodor Kocher Institute, Bern, Switzerland. [3]Walter Brendel Centre of Experimental Medicine, Ludwig Maximilians University, Munich, Germany. [4]Department for Molecular Medicine, Max-Planck Institute for Biochemistry, Martinsried, Germany. [5]DZHK (German Centre for Cardiovascular Research), Partner Site Munich Heart Alliance, Munich, Germany. [6]Joint Research Division Vascular Biology, Medical Faculty Mannheim (Centre for Biomedicine and Medical Technology Mannheim) and German Cancer Research Center (DKFZ–Zentrum für Molekulare Biologie der Universität Heidelberg Alliance), Heidelberg, Germany. [7]Institute for Cardiovascular Prevention, Ludwig Maximilians University, Munich, Germany. [8]Discovery Oncology, Pharma Research and Early Development, Roche Diagnostics GmbH, Penzberg, Germany.

Septic shock is characterized by increased vascular permeability and hypotension despite increased cardiac output. Numerous vasoactive cytokines are upregulated during sepsis, including angiopoietin 2 (ANG2), which increases vascular permeability. Here we report that mice engineered to inducibly overexpress ANG2 in the endothelium developed sepsis-like hemodynamic alterations, including systemic hypotension, increased cardiac output, and dilatory cardiomyopathy. Conversely, mice with cardiomyocyte-restricted ANG2 overexpression failed to develop hemodynamic alterations. Interestingly, the hemodynamic alterations associated with endothelial-specific overexpression of ANG2 and the loss of capillary-associated pericytes were reversed by intravenous injections of adeno-associated viruses (AAVs) transducing cDNA for angiopoietin 1, a TIE2 ligand that antagonizes ANG2, or AAVs encoding PDGFB, a chemoattractant for pericytes. To confirm the role of ANG2 in sepsis, we i.p. injected LPS into C57BL/6J mice, which rapidly developed hypotension, acute pericyte loss, and increased vascular permeability. Importantly, ANG2 antibody treatment attenuated LPS-induced hemodynamic alterations and reduced the mortality rate at 36 hours from 95% to 61%. These data indicate that ANG2-mediated microvascular disintegration contributes to septic shock and that inhibition of the ANG2/TIE2 interaction during sepsis is a potential therapeutic target.

Introduction

Constitutive ablation of the TIE2 receptor impairs vascular integrity during a midgestional stage of development (1, 2). Interestingly, these observations have been phenocopied by a heart-restricted ablation of the angiopoietin 1 (*Ang1*) gene (3). Loss of ANG1 (4) as well as endothelial overexpression of angiopoietin 2 (ANG2), antagonizing TIE2 (5), both induce vessel destabilization during development. Recent evidence suggests that increased destabilization and vascular regression in adult organisms occur by ANG2/TIE2–mediated phosphorylation of Ser910 of focal adhesion kinase (6, 7). ANG2 was shown to be upregulated in a variety of disease entities linked to systemic inflammation, hyperpermeability, and vessel destabilization: renal failure in patients with multiorgan disease, pulmonary leakiness leading to adult respiratory distress syndrome, and sepsis development have all been linked to increased ANG2 levels circulating in the blood (8–11). These findings raise the possibility that excess ANG2 critically affects the cardiovascular homeostasis during sepsis by disturbing the microvascular architecture, potentially by impairing endothelial/pericyte interaction. It has been shown previously that vascular permeability is controlled by pericytes in the blood-brain barrier (12). However, a role of pericytes controlling vascular integrity and blood pressure homeostasis during systemic inflammatory processes has not been studied.

In this paper, we investigated whether ANG2, when inducibly overexpressed in the endothelium or cardiomyocytes of mice, induces hyperpermeability, hypotension, and pericyte loss in vivo. Finally, we also investigated whether ANG2 inhibition is beneficial for pericyte investment and hemodynamic stability in a murine model of endotoxemia.

Results

First, we generated a mouse strain in which moderate human ANG2 (hANG2) expression was induced in endothelial cells in the absence of tetracyclines and could be switched off by the oral application of doxycycline (TIE2-tTA/TRE-hANG2 mice, referred to herein as EC-ANG2-on mice; Supplemental Figure 1; supplemental material available online with this article; doi:10.1172/JCI66549DS1). In the EC-ANG2-on state, mice displayed increased body weight (Supplemental Figure 2), edema (Figure 1A), and increased vascular diameters (Figure 1B). Moreover, permeability of ear vessels for the small molecule tracer TRITC-dextrane (4 kDa) was enhanced in EC-ANG2-on mice (Figure 1, C and D).

The rise in permeability conveyed by ANG2 (13) was previously attributed to its antagonism toward ANG1, a TIE2 ligand secreted by pericytes and promoting endothelial integrity (4,

Authorship note: Tilman Ziegler, Jan Horstkotte, and Claudia Schwab contributed equally to this work. Reinhard Fässler, Urban Deutsch, and Christian Kupatt are co–senior authors.

Conflict of interest: The authors have declared that no conflict of interest exists.

Citation for this article: *J Clin Invest.* 2013;123(8):3436–3445. doi:10.1172/JCI66549.

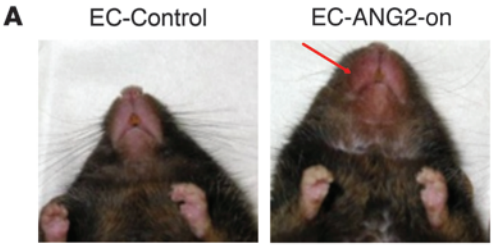

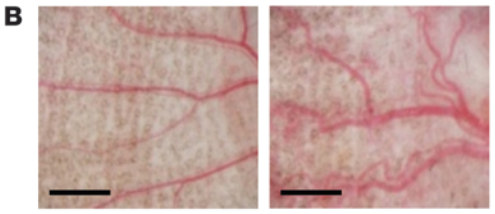

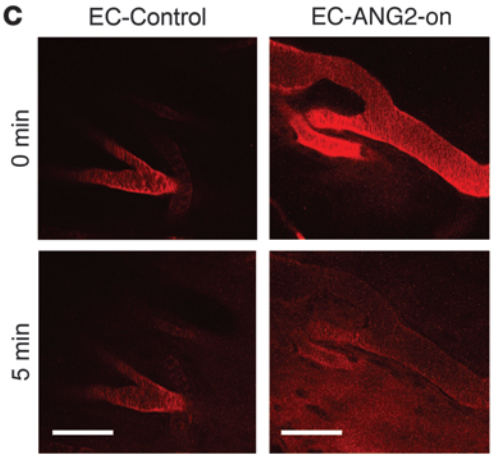

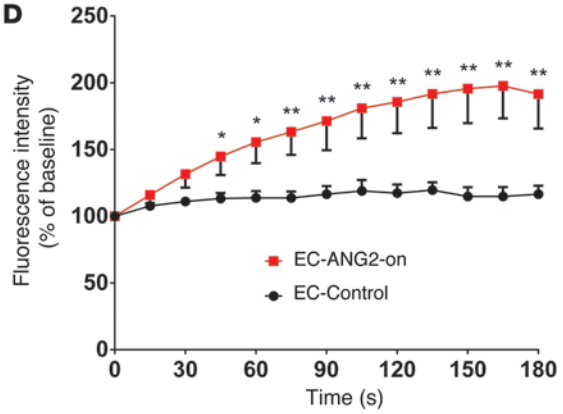

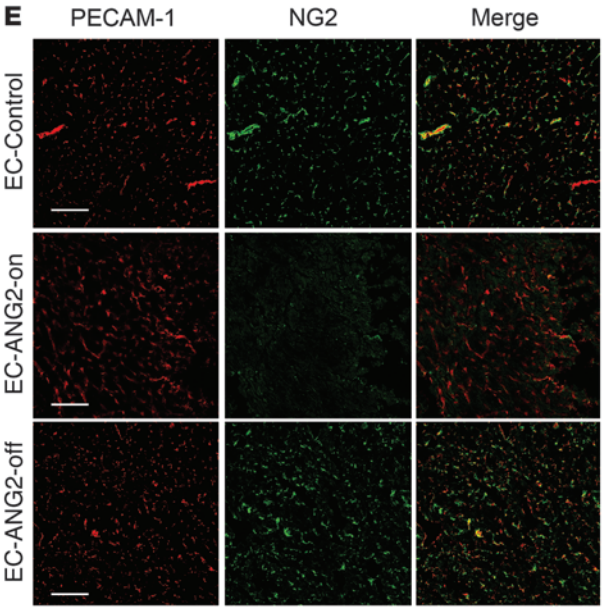

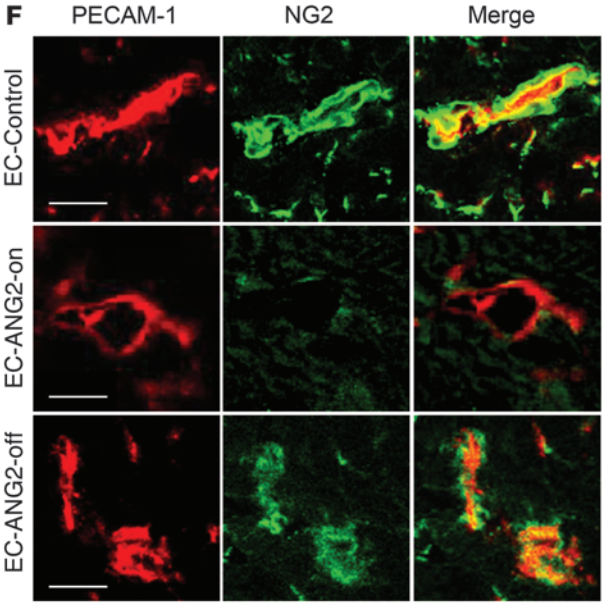

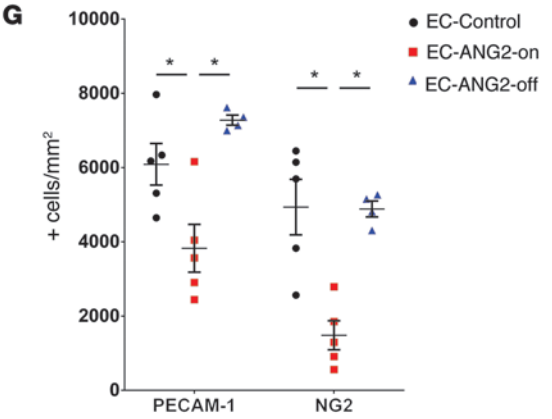

Figure 1
Endothelial ANG2 overexpression induces pericyte loss and increased vascular permeability. (**A**) Inducible endothelial ANG2-overexpressing mice (EC-ANG2-on mice) develop enlarged lips (red arrow), (**B**) enlarged ear vessels (scale bar: 200 μm), and (**C** and **D**) increased permeability for 4-kDa TRITC-dextran (scale bar: 50 μm; $n = 4$). (**E**–**G**) Cardiac capillary density (PECAM-1 staining) and pericyte coverage (NG2 staining) are decreased in EC-ANG2-on mice ($n = 5$ for EC-Control and EC-ANG2-on, $n = 4$ for EC-ANG2-off). Scale bar: 50 μm (**E**); 5 μm (**F**). *$P < 0.05$, **$P < 0.001$.

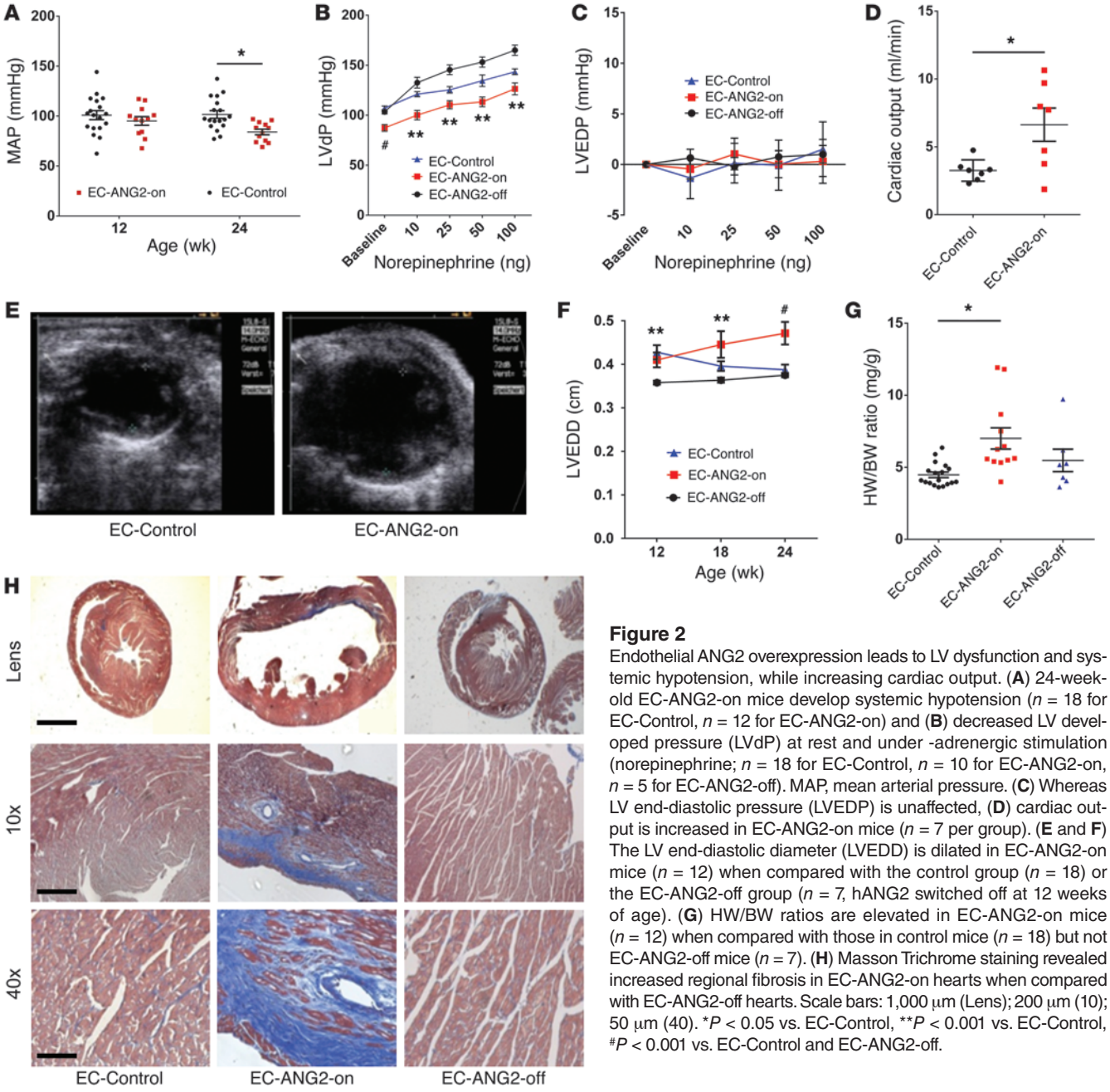

Figure 2

Endothelial ANG2 overexpression leads to LV dysfunction and systemic hypotension, while increasing cardiac output. (**A**) 24-week-old EC-ANG2-on mice develop systemic hypotension (n = 18 for EC-Control, n = 12 for EC-ANG2-on) and (**B**) decreased LV developed pressure (LVdP) at rest and under -adrenergic stimulation (norepinephrine; n = 18 for EC-Control, n = 10 for EC-ANG2-on, n = 5 for EC-ANG2-off). MAP, mean arterial pressure. (**C**) Whereas LV end-diastolic pressure (LVEDP) is unaffected, (**D**) cardiac output is increased in EC-ANG2-on mice (n = 7 per group). (**E** and **F**) The LV end-diastolic diameter (LVEDD) is dilated in EC-ANG2-on mice (n = 12) when compared with the control group (n = 18) or the EC-ANG2-off group (n = 7, hANG2 switched off at 12 weeks of age). (**G**) HW/BW ratios are elevated in EC-ANG2-on mice (n = 12) when compared with those in control mice (n = 18) but not EC-ANG2-off mice (n = 7). (**H**) Masson Trichrome staining revealed increased regional fibrosis in EC-ANG2-on hearts when compared with EC-ANG2-off hearts. Scale bars: 1,000 μm (Lens); 200 μm (10); 50 μm (40). $^{*}P < 0.05$ vs. EC-Control, $^{**}P < 0.001$ vs. EC-Control, $^{\#}P < 0.001$ vs. EC-Control and EC-ANG2-off.

14–16). Moreover, pericyte loss itself causes increased permeability in distinct vascular beds, e.g., the blood-brain barrier (12). Therefore, we investigated the possibility of pericyte loss in the hyperpermeable EC-ANG2-on state. Indeed, EC-ANG2-on hearts revealed a significant loss of pericytes, which coincided with lower capillary counts (Figure 1, E–G). Of particular note, doxycycline was applied at week 12 to switch off ANG2 formation, which was present since birth. This protocol entirely prevented the pericyte loss and capillary rarefaction at the 24-week time point (Figure 1, E–G). Moreover, recombinant adeno-associated virus ANG2 (rAAV.ANG2) transduction reduced the number of mural cells in the XLacZ4 mouse, which expresses β-galactosidase in mural cells (Supplemental Figure 2, A–C, and ref. 17).

We next analyzed the cardiovascular sequelae of the observed microvascular disturbance. Mean arterial pressure, obtained noninvasively by repetitive tail artery cuff measurements, decreased over time in the EC-ANG2-on mice (93 ± 3 mmHg at 12 weeks and 85 ± 3 mmHg at 24 weeks), significantly differing from that of controls at 24 weeks (101 ± 2 and 100 ± 2 mmHg, respectively, $P < 0.05$ at 24 weeks; Figure 2A). Consistently, LV developed pressure (Figure 2B) was significantly lower over a broad range of norepinephrine stimuli (from 10 to 100 ng boli), when assessed invasively by a pressure-tip catheter. The failure to mount a normal systolic blood pressure level was blunted by doxycycline-mediated inhibition of the previously active hANG2 expression at 12 weeks and until 24 weeks of age. In order to

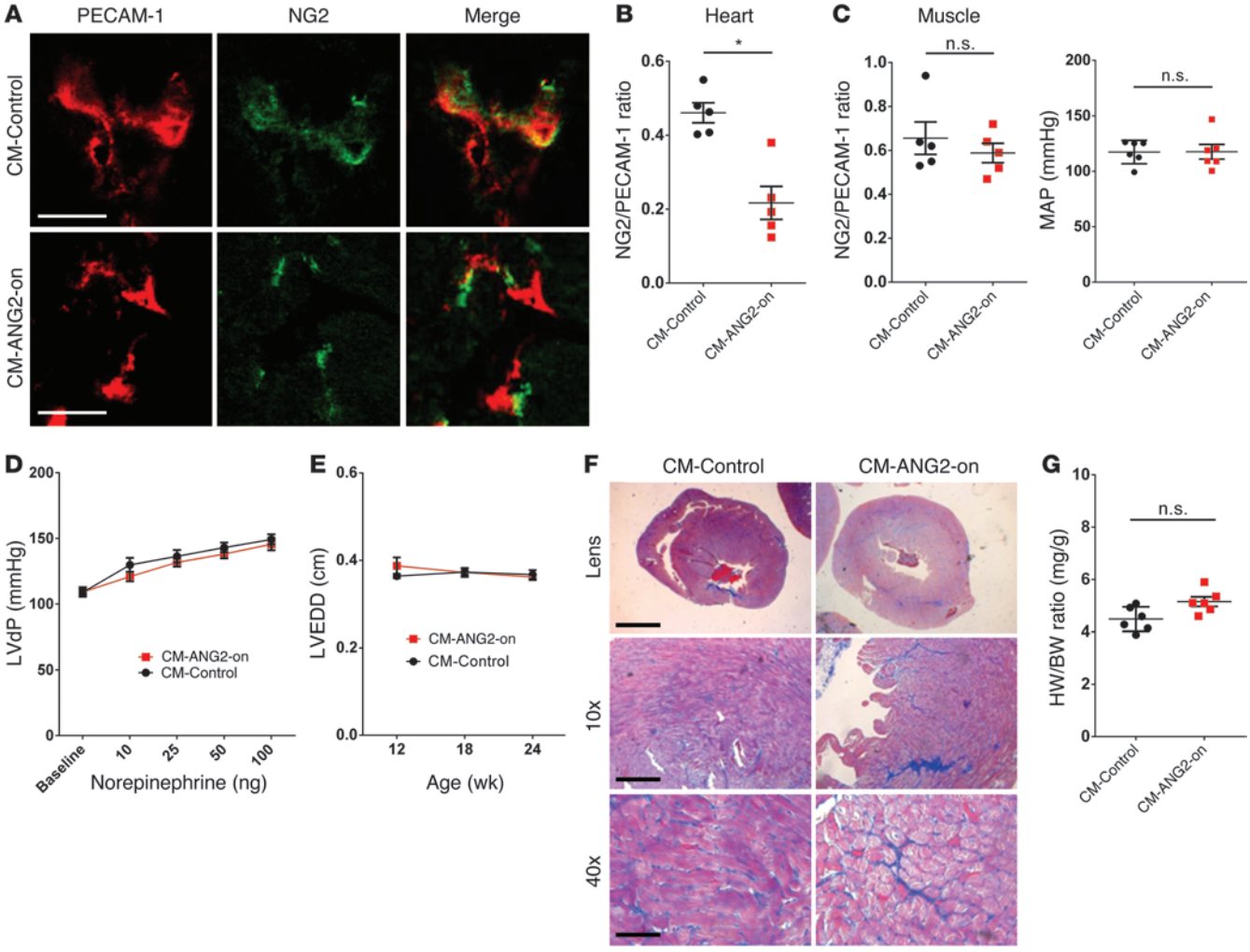

Figure 3

Cardiomyocyte-specific ANG2 overexpression does not induce peripheral microcirculatory and hemodynamic alterations. (**A** and **B**) Cardiomyocyte-specific ANG2 overexpression (CM-ANG2-on) reduces pericyte coverage (NG2 staining) of capillaries (PECAM-1 staining) in cardiac but not skeletal muscle (scale bar: 5 μm; $n = 5$). (**C**) Systemic mean arterial pressure ($n = 6$) and (**D**) LV developed pressure is normal in 24-week-old CM-ANG2-on mice ($n = 6$ per group). (**E**) CM-ANG2-on mice display normal LV end-diastolic diameter ($n = 6$). (**F**) Minimal fibrosis was detected in CM-ANG2-on hearts. Scale bars: 1,000 μm (Lens); 200 μm (×10); 50 μm (×40). (**G**) HW/BW ratio was unaffected in CM-ANG2-on mice ($n = 6$). *$P < 0.05$.

distinguish between a systolic pump failure of the heart and a hypercirculatory state due to peripheral resistance loss, we analyzed LV end-diastolic pressure and cardiac output. Of note, LV end-diastolic pressure did not differ among control hearts as well as EC-ANG2-on hearts and hearts of mice with endothelial ANG2 overexpression switched off (EC-ANG2-off mice) (Figure 2C). In contrast, cardiac output was significantly increased in the EC-ANG2-on mice (Figure 2D).

Reduced peripheral resistance and increased cardiac output are indicative of a hypercirculatory state, which leads to altered cardiac morphology. From 12 to 24 weeks of age EC-ANG2-on hearts displayed a progressive dilation of LV end-diastolic diameters (Figure 2, E and F). Switching off ANG2 at the 12-week time point prevented a further LV end-diastolic diameter increase over time (Figure 2F). Moreover, an increased heart weight to body weight (HW/BW) ratio indicated a gain of heart muscle mass in the EC-ANG2-on state, when compared with that of control hearts (Figure 2G). EC-ANG2-off hearts were indistinguishable from control hearts and displayed a strong trend toward a lower HW/BW ratio compared with EC-ANG2-on hearts ($P = 0.07$; Figure 2G). Histologically, fibrosis was found in a patchy fashion in EC-ANG2-on hearts (Figure 2H and Supplemental Figure 2E) but neither in control hearts nor in EC-ANG2-off hearts. Taken together, pan-endothelial overexpression of ANG2 induces increased microvascular permeability and pericyte loss, associated with hypotensive hypercirculation and pathological cardiac hypertrophy.

We next asked whether the cardiac phenotype was caused by local, heart-specific or systemic, remote microvascular alterations. Therefore, we assessed the phenotype of a cardiomyocyte-restricted ANG2 overexpression (CM-ANG2-on) by using α-MHC–restricted expression of tTA. Of note, although heart-specific pericyte loss was observed in CM-ANG2-on mice (Figure 3, A and B, and Supplemental Figure 3A), skeletal muscle areas revealed

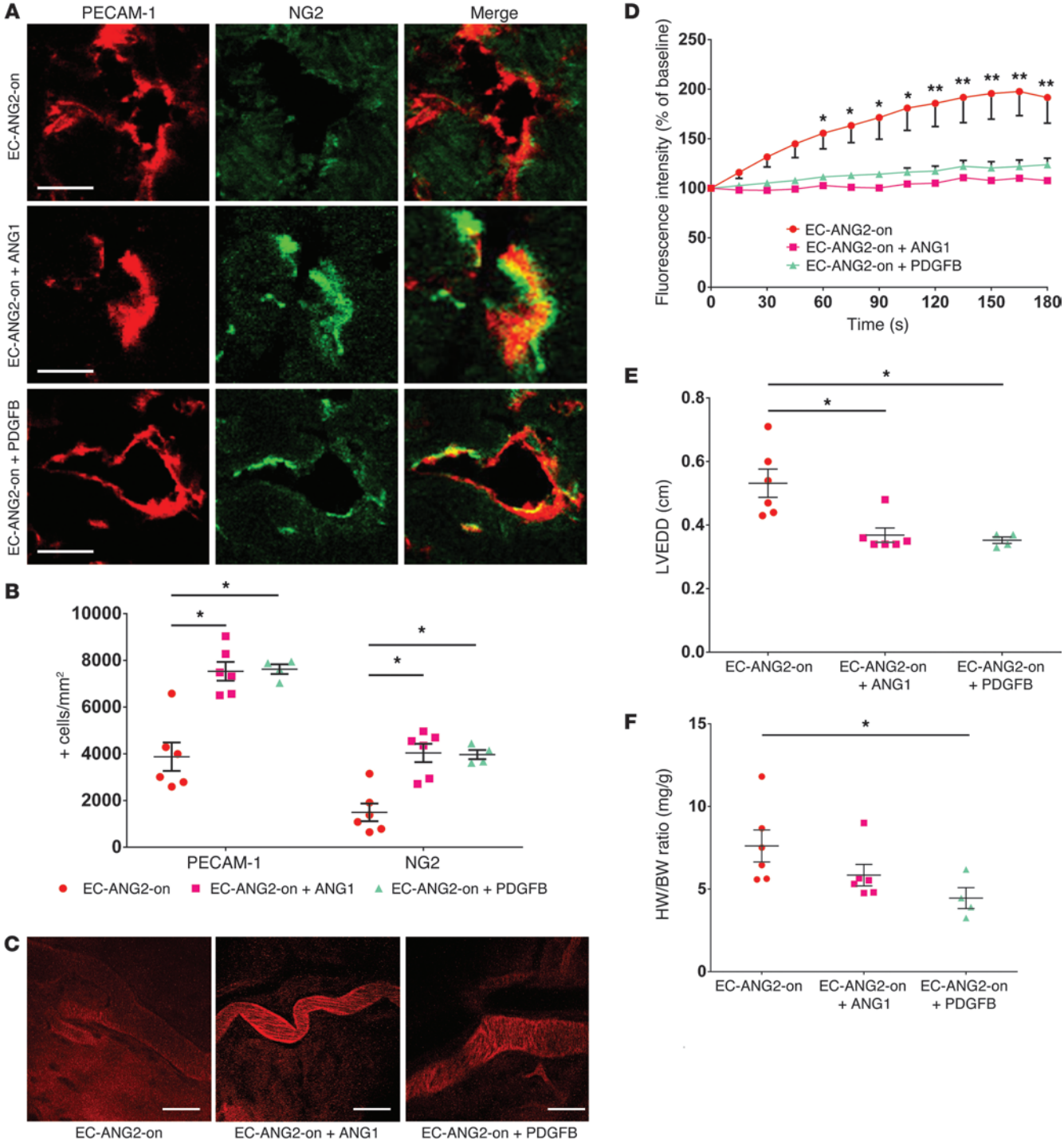

Figure 4

EC-ANG2-on induced microcirculatory and hemodynamic alterations are antagonized by ANG1 and PDGFB. (**A** and **B**) Pericyte loss (NG2 staining) and capillary rarefaction (PECAM-1 staining) in EC-ANG2-on mice are blocked by rAAV-transduced ANG1 and PDGFB, respectively (scale bar: 5 μm; $n = 6$ per group except PDGFB [$n = 4$]). (**C** and **D**) rAAV-transduced ANG1 and PDGFB normalized permeability in the ear vasculature of EC-ANG2-on mice (scale bar: 50 μm). (**E**) rAAV-transduced expression of ANG1 and PDGFB in 24-week-old EC-ANG2-on mice prevents an increase of LV end-diastolic diameter and (**F**) a reduction in HW/BW ratio in the case of PDGFB. $n = 6$ per group except EC-ANG2-on and PDGFB ($n = 4$). $^*P < 0.05$, $^{**}P < 0.001$.

a normal ratio of pericyte/capillary cells (Figure 3B). Cardiac-restricted ANG2 overexpression did not alter systemic blood pressure (Figure 3C) or LV systolic function and diameter (Figure 3, D and E) over time. Consistently, no increase in fibrosis was found in hearts from this condition (Figure 3F and Supplemental Figure 3B), and HW/BW ratio was normal in CM-ANG2-on mice (Figure 3G). Wild-type hearts treated with cardiotropic rAAV at a dose transducing heart but not peripheral muscle phenocopied the hemodynamic results (Supplemental Figure 3, D–G, and Supplemental Methods). Thus, cardiomyocyte-specific ANG2 overexpression, though altering cardiac microvascular architecture, did not replicate the pan-endothelial EC-ANG2-on hypercirculatory state inducing cardiac remodeling.

A central mechanism of ANG2 signaling is to displace ANG1 from binding to the TIE2 receptor kinase, thereby altering endothelial/pericyte interaction, attachment to the extracellular matrix, and, consecutively, permeability (18, 19). In light of these properties, we devised two strategies to rescue the phenotype of ANG2-induced hypercirculatory cardiomyopathy. First, we transduced mice with intravenous rAAV.ANG1 injection, in order to restore the physiological ratio of ANG1 and ANG2, albeit on a higher level (Supplemental Figure 4A). Second, we attempted to reattract pericytes to the capillaries, which had lost pericytes after ANG2 induction, via intravenous injection of an rAAV-transducing PDGFB (Supplemental Figure 4B), an essential ligand for pericyte attraction (20). We found that rAAV.ANG1 and rAAV.PDGFB applied at 12 weeks of age both sufficed to increase the number of pericytes per mm^2 of muscle area in heart muscle by 24 weeks of age (Figure 4, A and B, and Supplemental Figure 4C). The normalization of the ANG1/ANG2 balance as well as restoration of pericyte coverage by PDGFB normalized permeability of ear capillaries in EC-ANG2-on mice (Figure 4, C and D). Moreover, cardiac enlargement (Figure 4E), indicating cardiac remodeling in EC-ANG2-on mice, was prevented after rAAV.ANG1 or rAAV.PDGFB application. HW/BW ratios were significantly reduced by rAAV.PDGFB and displayed a strong trend toward reduction after rAAV.ANG1 transduction ($P = 0.07$; Figure 4F). In summary, forced expression of ANG1, which competes with ANG2 for TIE2, and of PDGFB, which counteracts ANG2-induced pericyte loss, both efficiently block ANG2-induced microvascular and hemodynamic disintegration.

The hyperpermeability and hypercirculatory state of the EC-ANG2-on mice, caused by disturbance of the peripheral microcirculation, bears strong resemblance to the cardiovascular alteration found in sepsis. Therefore, we induced a systemic inflammation in wild-type mice and assessed the relevance of ANG2-induced pericyte loss and hyperpermeability for the hemodynamic destabilization and mortality. i.p. injection of 20 mg/kg LPS sufficed to induce a robust upregulation of TNF-α and IL-6 (Figure 5, A and B). Pretreatment with a recombinant anti-ANG2 antibody, LC10, did not prevent the increase in levels of TNF-α and IL-6 seen in control antibody–treated animals (Figure 5, A and B). However, ANG2 antibody pretreatment blocked the LPS-induced permeability increase of the ear vasculature (Figure 5C). Moreover, ANG2 antibody application blunted the loss of pericytes observed in the early course of endotoxemia development (12 hours), both in the heart (Figure 5, D–F) as well as in peripheral muscles (Figure 5G), without significantly affecting neutrophil recruitment at this time point (Supplemental Figure 5A).

To assess the possibility that microvascular disintegration affects hemodynamic stability, causing septic shock, we analyzed the blood pressure in LPS-treated wild-type mice. Systemic hypotension, a hallmark of septic shock, was found at the same time point as microvascular disintegration (12 hours; data not shown) and persisted at 24 hours (Figure 5H). This hemodynamic alteration sufficed to inflict a high mortality rate, which progressed to 95% at 36 hours. Anti-ANG2 antibody treatment with either of two different antibodies, LC10 and LC06, was capable of reducing this rate significantly (Figure 5I). In contrast, EC-ANG2-on mice, which already displayed an edematous phenotype before LPS challenge, succumbed faster to the systemic inflammation than age-matched controls (Supplemental Figure 5B). A similar finding was obtained while applying LC10 in an alternate sepsis model inflicted by cecal puncture and ligation (Figure 5J). The observation that intravenous anti-ANG2 antibody application increased microvascular integrity, blood pressure, and survival points to a causative role of ANG2 for crucial microvascular alterations in sepsis.

Finally, we tested whether increasing the PDGFB level stabilizes pericytes and thus antagonizes microvascular and hemodynamic sequelae of endotoxemia. Pretreatment of wild-type mice with rAAV.PDGFB did not affect the level of inflammation (Supplemental Figure 6A) but prevented the rise in vascular permeability in the ear observed after LPS application (Supplemental Figure 6B). As hypothesized, pericyte loss was blunted by rAAV.PDGFB in the coronary (Supplemental Figure 6, C and D) as well as in the peripheral microcirculation (Supplemental Figure 6E). Moreover, blood pressure was significantly higher than that in rAAV.LacZ-treated mice (Supplemental Figure 6F). Survival analysis revealed a better outcome in the case of rAAV.PDGFB at 24 and 36 hours than after rAAV.LacZ pretreatment (Supplemental Figure 6G). Thus, PDGFB provides stabilization of pericyte attachment to the capillary network, a step sufficient to prevent increased permeability as well as hemodynamic dysregulation following septic stimulation.

Discussion

In this study, we found that increased endothelial ANG2 expression induces hyperpermeability and pericyte loss (Figure 1). In addition, EC-ANG2-on mice displayed a drop in systolic blood pressure (Figure 2, A and B), despite an increased cardiac output (Figure 2D), indicating a hypercirculatory state. LV dilation, hypertrophy, and fibrosis were detected after 6 months of ANG2 overexpression, reflecting compensatory cardiac remodeling (Figure 2, E–H). The notion that ubiquitous microvascular disintegration causes the hypercirculatory state was strengthened by the striking difference between the EC-ANG2-on and the CM-ANG2-on mouse strains, the latter displaying no apparent hemodynamic alterations despite cardiac pericyte loss (Figure 3). The EC-ANG2-on phenotype was rescued by systemic application of rAAV.ANG1 or rAAV.PDGFB, indicating that both TIE2 signaling and pericyte recruitment are of relevance for the EC-ANG2-on phenotype (Figure 4). These observations are replicated by the in vitro analysis of pericyte recruitment to cultured endothelial cells, which is impaired after ANG2 transfection and rescued by ANG1 and PDGFB (Supplemental Figure 7).

The potential of ANG2 to disrupt vessel formation in the developing embryo was initially reported by Maisonpierre et al. (5). While in ANG2-transgenic E9.5 embryos a more severe lack of PECAM-1–positive cells is observed, the phenotype is qualitatively

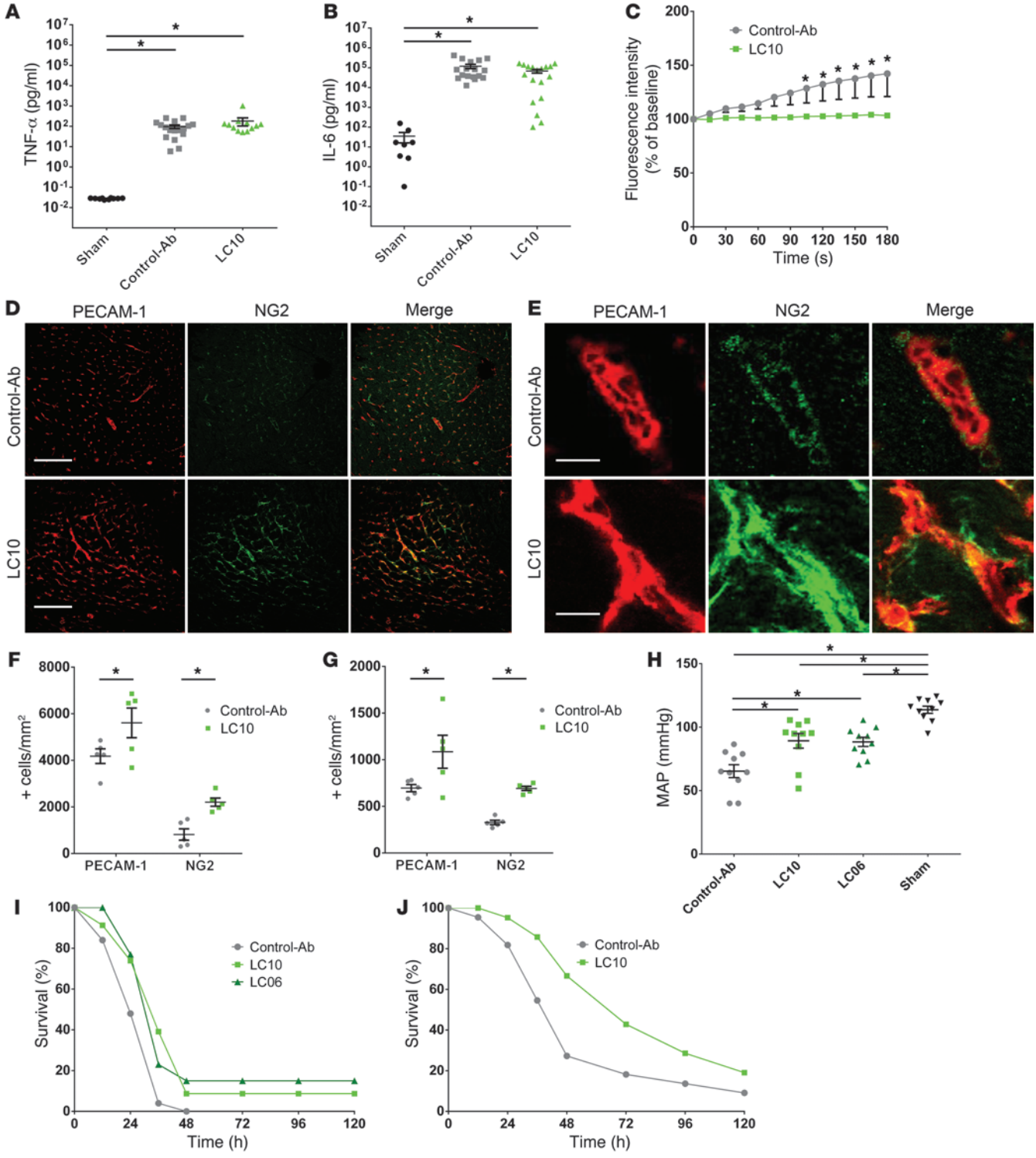

Figure 5

Inhibition of ANG2 reduces pericyte loss and mortality in a sepsis model. (**A**) TNF-α and (**B**) IL-6 levels increase 12 hours after i.p. injection of LPS in control mice and mice treated with anti-ANG2 antibody (LC10). (**C**) LC10 treatment prevents increased microcirculatory permeability 12 hours after LPS injection (representative result of $n = 3$). (**D** and **E**) LC10 treatment prevents pericyte loss and capillary rarefaction in coronary microcirculation. Scale bar: 100 μm (**D**); 5 μm (**E**). (**F**) Mice treated with ANG2 antibody (LC10) display increased capillary density (PECAM-1 staining) and pericyte coverage (NG2 staining) in myocardial and (**G**) peripheral microcirculation of quadriceps muscle ($n = 5$ per group). (**H**) Mean blood pressure after 12 hours ($n = 10$ per group) and (**I**) survival were increased following sepsis induction in mice pretreated with ANG2 antibodies ($n = 25$ for Control-Ab, $n = 23$ for LC10, $n = 13$ for LC06; log-rank $P = 0.0044$ for LC10, $P = 0.017$ for LC06). (**J**) LC10 treatment is able to reduce mortality in a cecal ligation and puncture model of sepsis ($n = 22$ for Control-Ab, $n = 21$ for LC10; log-rank $P = 0.036$). *$P < 0.05$.

similar to that of the EC-ANG2-on mice in our study (Figure 1, E–G). Capillary regression and pericyte loss are also present in our endotoxemia model 12 hours after LPS injection (Figure 5), indicating that microcirculatory disruption is a cause for the hyperpermeable and hypercirculatory state. ANG2 levels are increased in this state and have been established as a prognostic biomarker for identification of the patient group with the highest mortality rates (21). Although antagonism of ANG2, e.g., by increasing ANG1 levels, has been performed successfully in sepsis (22, 23), we could show a significant effect of ANG2 inhibition for survival in endotoxemia/sepsis for the first time. In our study, the anti-ANG2 antibody did not attenuate the overall level of inflammation and endothelial activation in a model of LPS-induced endotoxemia (Figure 5, A and B, and Supplemental Figure 5A), as opposed to other antiinflammatory strategies directly affecting the LPS/TLR4–mediated signaling pathways, such as hepcidin (24).

At first sight, a contradictory result comes from Tzepi and coworkers, who reported that hANG2 pretreatment attenuated liver TNF-α secretion upon *Pseudomonas aeruginosa* infection, providing a survival advantage, which was not reproduced in TNF-α–deficient mice. However, ANG2 pretreatment did not provide a survival advantage after LPS treatment, rather revealing a trend toward lower survival (25). Moreover, in the study by Tzepi et al., pretreatment with 25 μg/kg human recombinant ANG2 was exogenously applied, differing from our strategy of inhibition of endogenous ANG2 activity upon LPS endotoxemia (Figure 5I). It is noteworthy that chronic ANG2 upregulation in the EC-ANG2-on mice further decreased survival after LPS endotoxemia in our study (Supplemental Figure 5B), pointing to a potential difference of chronic versus acute ANG2 upregulation.

The impact of ANG2 on the hemodynamic status required pan-endothelial exposure such as in the EC-ANG2-on model (Figure 2) and was absent in cardiac-restricted ANG2-overexpressing mice (Figure 3). Earlier studies demonstrated that ANG2 release from Weibel-Palade bodies is induced by increased endothelial stretch, which occurs during hypertension (26), potentially counteracting the hypertensive alterations. Accordingly, previous work by Reiss and coworkers suggests that ANG2 overexpression also affects smooth muscle cell recruitment directly or indirectly (via disturbed microvessel maturation) in a murine hind limb ischemia model (27). Recent evidence points to the possibility of a direct effect of pericytes on the vascular tone, e.g., after traumatic brain injury (28).

Of note, nitric oxide synthase inhibition by oral L-NAME application was also capable of entirely preventing hypotension and subsequent cardiac remodeling of the EC-ANG2-on phenotype (mean arterial pressure 100 ± 8 mmHg vs. 84 ± 3 mmHg in the EC-ANG2-on group, HW/BW ratio 4.82 ± 0.14 vs. 7.21 ± 1.10 in the EC-ANG2-on group). Nitric oxide release upon VEGF-A stimulation (29, 30) mediates microvascular permeability (31) and hypotension (32). Ahmed et al. reported that a single administration of an adenovirus encoding for ANG2 reduces atherosclerosis progression in *Apoe*$^{-/-}$ mice fed with Western diet, an effect blocked by nitric oxide synthase inhibition (33). Thus, nitric oxide and ANG2 signaling display several functional similarities. However, recruitment of mural cells (pericytes and smooth muscle cells) after induction of murine hind limb ischemia requires nitric oxide (34), whereas in our study, ANG2 mediates endotoxemia-induced loss of pericytes (Figure 5, D–G). This difference may either be related to varying pathophysiologic stimuli (ischemia vs. endotoxemia) or imply an alternate behavior of pericytes upon ANG2 or nitric oxide stimulation.

Interestingly, the close connection of microvascular integrity and blood pressure homeostasis has also been observed in *Pdgfb*$^{ret/ret}$ transgenic mice. Here, a variant lacking the retention motif of PDGFB required for association with extracellular matrix causes a similar phenotype: besides pericyte loss (35) and capillary rarefaction, cardiac output and heart weight increased, indicating a hypercirculatory state (36). In the EC-ANG2-on strain, which did not display altered PDGFB expression in heart and muscle tissue (Supplemental Figure 2F), hyperpermeability and cardiac remodeling were prevented by using a long-lasting rAAV.PDGFB vector, which recruited pericytes to capillaries (Figure 4). Consistently, an rAAV.PDGFB vector was capable of blunting mortality during LPS-induced systemic inflammation, similar to anti-ANG2 antibodies (Supplemental Figure 6). These findings support the role of pericytes for control of vascular permeability and hemodynamic stability.

In summary, pan-endothelial ANG2 overexpression induces a profound phenotype, featuring hyperpermeability and pericyte loss as well as hypercirculatory hypotension, subsequently leading to cardiac hypertrophy and fibrosis. These alterations were prevented by increasing ANG1, an antagonist of ANG2, or by PDGFB, providing pericyte recruitment. Moreover, ANG2 inhibition and PDGFB overexpression significantly reduced microvascular alterations as well as hypotension and mortality in LPS-induced systemic inflammation. Thus, ANG2-induced pericyte loss exerts a causative role in the hemodynamic alterations, culminating in septic shock and making ANG2 a worthwhile therapeutic target in these pathologies.

Methods

Transgenic mice. Transgenic mice were generated following standard procedures described previously (37). We used the endothelial cell–specific tetracycline-regulatable transactivator transgenic (activator) mouse line, B6JTg(TIE2-tTA)3Udeu (TIE2-tTA) (38), and a responder mouse line carrying a chicken β-globin insulator flanked bidirectional construct coding for hANG2 and a GFP reporter, B6J-Tg(TRE-hANG2)5Udeu (TRE-hANG2) (Supplemental Figure 1A). Breeding stock for generation of double transgenic mice was kept on doxycycline-containing food until pups were delivered. Then, endothelial cell–specific expression of hANG2 (EC-ANG2-on; Supplemental Figure 1) was induced by stopping the feeding of doxycycline at birth in all groups (doxycycline [Sigma-Aldrich]; 100 mg/kg chow). In a subgroup (EC-ANG2-off), doxycycline was reapplied from 12 to 24 weeks of age, terminating the transgenic overexpression. In double transgenic mice of the Tg(TRE-hANG2)5Udeu line, no expression of GFP is detectable from the bidirectional construct in the absence of doxycycline. Mice were housed under specific pathogen–free conditions in either individually ventilated or filter top cages. The genotype of mice was confirmed by PCR using tail biopsies before and after the experiments. Alternately, an α-MHC-tTA activator line (FVB.Cg-Tg [Myh6-tTA]6Smbf/J; The Jackson Laboratory) was used to generate double transgenic mice expressing hANG2 in a cardiomyocyte-restricted fashion in the absence of tetracycline (CM-ANG2-on mice) (39).

For analyses, double transgenic mice were compared with single transgenic littermate control animals (off doxycycline). All animal procedures were performed in accordance with the animal protection law of the Kanton Bern, Switzerland, the Swiss legislation on the protection of animals, and approved by the respective government authorities.

Genotyping. Offspring from matings of hemizygous TIE2-tTA and TRE-hANG2 mice were biopsied at weaning age, and tissue lysates were analyzed by PCR for the presence of the respective transgenes. Primers (hANG2 FW3 [5′-TGCCACGGTGAATAATTCAG-3′] and hANG2 REV3 [5′-TTCTTCTTTAGCAACAGTGGG-3′]) were used for the TRE-hANG2

allele PCR, with 35 cycles of 30 seconds at 94°C, 30 seconds at 54°C, and 30 seconds 72°C. The resulting PCR product was 150 bp in size. For both tTA transgenic alleles, a product of 535 bp in size was amplified by 35 cycles of 30 seconds at 94°C, 45 seconds at 63°C, and 45 seconds at 72°C, using the primers tTA-FW2 (5′-GACGCCTTAGCCATTGAGATG-3′) and tTA-Rev2 (5′-CAGTAGTAGGTGTTTCCCTTTCTTC-3′).

Chronic mouse protocol. At 12 weeks of age, EC-ANG2-on mice, CM-ANG2 on mice, and controls underwent baseline assessment of echocardiographic imaging using a standard ultrasound system combined with a 15 MHz transducer (Acuson Sequoia 512 and Acuson 15L8 Transducer, Siemens AG), and noninvasive blood pressure was measured using the CODA system (Kent Scientific). Thereafter, EC-ANG2-on mice were treated with doxycycline, rAAV.PDGFB (5×10^{12} virus particles), or rAAV.ANG1 virus (5×10^{12} virus particles) where indicated. An additional group of C57BL/6 mice received 1×10^{12} virus particles in the tail vein for cardiomyocyte-specific transduction (Supplemental Figure 3, D–G, and Supplemental Methods). Echocardiographic imaging was repeated at 18 and 24 weeks followed by a LV catheterization using a Millar-Tip catheter (SPR-671, Millar Instruments) to determine the LV developed pressure and LV end-diastolic pressure (40). For evaluation of pressure-volume relationships, an impedance-micromanometer catheter (Millar Instruments) was placed the same way, and pressure-volume loops were recorded (41). Raw conductance volumes were corrected for parallel conductance by the hypertonic saline dilution method.

Sepsis protocol. C57BL/6J mice (Charles River) were injected with anti-ANG2 antibody (LC10 or LC06, Roche, 20 mg/kg i.p.) or a control antibody (AP112, Millipore, 20 mg/kg i.p.) 24 hours before induction of the systemic inflammation using 20 mg/kg LPS from *E. coli* (L2880, Sigma-Aldrich). The scoring system used to assess the clinical severity is described in Supplemental Table 1. Endotoxemia severity was assessed as described above at 6, 12, 24, and 36 hours in a blinded fashion. A score of 20 or higher was equated with the death of the animal. Noninvasive blood pressure was measured at 12 and 24 hours as outlined above. Blood plasma samples were taken at 12 hours, and permeability was assessed at 6 hours after induction of systemic inflammation (see below).

For cecal ligation and puncture, C57BL6/J mice were pretreated with 20 mg/kg antibody i.p. 24 hours prior to ligation of 1 cm of cecum followed by 3 punctures (23-gauge needle).

Permeability measurement. Multiphoton microscopy was performed with a TriMScope (LaVision BioTec) in single point scanning mode. 860 nm wavelengths were used to simultaneously excite TRITC fluorescence (recorded with 580/60-nm filter) and second harmonic generation of collagen (447/60-nm filter) (42). In analgosedation (see above), a mouse ear region was placed perpendicular to the optical axis on the microscopic stage. A suitable area of the ear was roughly localized by 1-photon background fluorescence and precisely defined using the second harmonic generation signal. A 3D movie was recorded, with a 200- × 200- × 36-μm stack (10 planes with 534 pixels squared each) being recorded every 15 seconds for 5 minutes. After recording the first data point, 750 μg TRITC-dextrane, with a molecular weight of 4 kDa (T1037, Sigma-Aldrich), was injected in 150 μl PBS. For data analysis, 3 areas were marked in direct contact to the vessel with an average size of 100 μm^2, and mean gray values (MGVs) were recorded in every picture using ImageJ imaging software (W.S. Rasband, US National Institutes of Health, http://imagej.nih.gov/ij/). Extravascular fluorescence at the time point of maximal intravascular fluorescence (in 3 different measurements after an average of 15 to 45 seconds after injection of TRITC-dextrane) was set as the starting point for the measurement and defined as 100% extravascular fluorescence. Changes in MGVs over time were calculated as the percentage of MGV at the starting point.

Virus production. The rAAV.hANG1, rAAV.hPDGFB, rAAV.hANG2, and rAAV.LacZ vectors were produced in U293 cells and purified with standard cesium sedimentation as previously described (43). Viral titers were determined using real-time PCR against the bGH 3′-untranslated region of the virally encoded transcript. The forward primer sequence was 5′-TCTAGTTGCCAGCCATCTGTTGT-3′, and the reverse primer sequence was 5′-TGGGAGTGGCACCTTCA-3′. Trans and helper plasmids were provided by James M. Wilson, University of Pennsylvania, Philadelphia, Pennsylvania, USA. Real-time PCR was used for virus detection in transfected mouse tissue. Primer sequences for human *ANG1* mRNA were forward 5′GGCCACAAGCATCAAACCAC and reverse 5′AATGGACTGGGAAGGGAACC; primer sequences for human *PDGFB* mRNA were forward 5′CCTCATAGACCGCACCAA and reverse 5′CGCACAATCTCGATCTTTCT; primer sequences for ANG2 were forward 5′TAGCATCAGCCAACCAGGAA and reverse 5′TAGTACTGTCCATTCAAGTT; and primer sequences for GAPDH were forward 5′ACCAGGAAATGAGCTTGACA and reverse 5′TCTTGGGCTACACTGAGGAC. Real-time PCR was performed using SYBR Green (Bio-Rad) for 40 cycles (30 seconds at 95°C, 30 seconds at 58°C, 30 seconds at 72°C) in an iQ-Cycler (Bio-Rad).

ANG2 antibody generation. Binding domains of the anti-ANG2 antibodies LC10 (RO5485202) and LC06 (RO5314193) were obtained from human antibody libraries, and the obtained VH and VL regions were maturated and then fused to the constant part of a human IgG1 antibody. The desired genes were generated by gene synthesis (GeneArt), PCR amplified, and cloned into suitable expression vectors. Variants of expression plasmids for transient expression in the HEK293-F system (Invitrogen) were applied for the expression of the described antibodies.

In order to study the effects of ANG2 and the respective antibodies on TIE2 downstream signaling, we have generated a HEK293 clone stably transfected with human TIE2. Stimulation with ANG2 or ANG1 results in phosphorylation of TIE2 in these cells. Subsequently, the ability of the identified antibodies to interfere with ANG2- and ANG1-mediated TIE2 phosphorylation was examined. LC06 has been described previously (44). LC10 showed a dose-dependent interference with ANG2-stimulated TIE2 phosphorylation, with an EC_{50} value of 3 nM. There was no interference with ANG1-stimulated TIE2 phosphorylation.

To further assess the selectivity of the ANG2 antibody, surface plasmon resonance was used. The Fab of RO5485202 was immobilized on the surface of a C1 SPR Chip. Fixed concentrations of hANG2 (multimeric) were preincubated together with increasing concentrations of the corresponding (immobilized) antibody and injected onto the flow cells. The K_d was calculated by plotting the concentrations of free hANG2 against the antibody concentrations (affinity in solution). The SPR data showed 10 nM affinity of RO5485202 for human and mouse ANG2 and no binding to human and mouse ANG1, confirming the selectivity of the antibody for ANG2.

Histological analysis and ELISA. Organs for histological analysis were embedded in Tissue-Tek OCT Compound (Sakura Finetek), and 8-μm sections were prepared using a cryotome. Sections were fixed with 4% paraformaldehyde and afterward blocked with 3% bovine serum albumin 0.1% Triton-X in PBS for 1 hour at room temperature. Primary antibodies used were CD31/PECAM-1 (BD Biosciences) and NG2 (Millipore). After washing with PBS, sections were incubated in appropriate fluorescent secondary antibodies (1:500) in PBS for 1 hour at room temperature. ELISAs from blood samples were performed using Quantikine ELISA Kits for murine IL-6 (R&D Systems) and murine TNF-α (R&D Systems) according to the respective protocols.

Statistics. Data are given as mean ± SEM. Differences among several groups were tested using ANOVA and Student Newman Keul's post-hoc analysis. $P < 0.05$ was considered statistically significant. Differences in survival curves were analyzed with the log-rank test (Kaplan-Meier survival). All data were assessed using the SPSS software package (version 20.0; http://www.spss.com).

Study approval. All animal experiments were approved by the Bavarian Animal Care and Use Committee (AZ 211-2531-2531-28-08 and AZ 55.2-1-54-2531-165-11) and conformed to the Guide for the Care and Use of Laboratory Animals published by the NIH (NIH publication no. 85-23, revised 1996).

Acknowledgments

This work was supported by the Deutsche Forschungsgemeinschaft (DFG, KU 1019/11-1/2 to C. Kupatt, DFG De 506/3-1 and 3-2 to U. Deutsch, and WE 1913/11-2 to C. Weber), the DZHK, and the German Ministry of Education and Research (BMBF) (to C. Kupatt, C. Weber, U. Pohl, W.M. Franz, and R. Fässler) as well as the Legerlotz-foundation (to C. Kupatt, J. Hu, and T. Ziegler) and FöFoLe grants (to J. Hu, V. Pfetsch, and K. Weinmann). We wish to thank Cuong Kieu, Elisabeth Raatz, Natasha Buchs, and Albert Witt for excellent technical assistance and Jörg Thomas Regula for antibody generation. We owe thanks to the animal caretakers: Svetlozar Tsonev, Isabelle Wymann, and Kerstin Blank. U. Deutsch acknowledges the support of Britta Engelhardt.

Received for publication August 24, 2012, and accepted in revised form May 6, 2013.

Address correspondence to: Christian Kupatt, Medizinische Klinik und Poliklinik I, Klinikum Großhadern der Ludwig Maximilians Universität, Marchioninistr. 15, 81377 Munich, Germany. Phone: 49.89.7095.6092; Fax: 49.89.7095.6075; E-mail: christian.kupatt@med.uni-muenchen.de.

1. Dumont DJ, et al. Dominant-negative and targeted null mutations in the endothelial receptor tyrosine kinase, tek, reveal a critical role in vasculogenesis of the embryo. *Genes Dev.* 1994;8(16):1897–1909.
2. Sato TN, et al. Distinct roles of the receptor tyrosine kinases Tie-1 and Tie-2 in blood vessel formation. *Nature*. 1995;376(6535):70–74.
3. Jeansson M, et al. Angiopoietin-1 is essential in mouse vasculature during development and in response to injury. *J Clin Invest.* 2011; 121(6):2278–2289.
4. Suri C, et al. Requisite role of angiopoietin-1, a ligand for the TIE2 receptor, during embryonic angiogenesis. *Cell*. 1996;87(7):1171–1180.
5. Maisonpierre PC, et al. Angiopoietin-2, a Natural Antagonist for Tie2 That Disrupts in vivo Angiogenesis. *Science*. 1997;277(5322):55–60.
6. Thomas M, et al. Angiopoietin-2 stimulation of endothelial cells induces alphavbeta3 integrin internalization and degradation. *J Biol Chem.* 2010;285(31):23842–23849.
7. Felcht M, et al. Angiopoietin-2 differentially regulates angiogenesis through TIE2 and integrin signaling. *J Clin Invest.* 2012;122(6):1991–2005.
8. Parikh SM, et al. Excess circulating angiopoietin-2 may contribute to pulmonary vascular leak in sepsis in humans. *PLoS Med.* 2006;3(3):e46.
9. Kumpers P, et al. Angiopoietin-2 in patients requiring renal replacement therapy in the ICU: relation to acute kidney injury, multiple organ dysfunction syndrome and outcome. *Intensive Care Med.* 2010;36(3):462–470.
10. Alves BE, et al. Imbalances in serum angiopoietin concentrations are early predictors of septic shock development in patients with post chemotherapy febrile neutropenia. *BMC Infect Dis.* 2010;10:143.
11. van der Heijden M, van Nieuw Amerongen GP, Van Hinsbergh VW, Groeneveld AB. The interaction of soluble Tie2 with angiopoietins and pulmonary vascular permeability in septic and nonseptic critically ill patients. *Shock*. 2010;33(3):263–268.
12. Armulik A, et al. Pericytes regulate the blood-brain barrier. *Nature*. 2010;468(7323):557–561.
13. Roviezzo F, et al. Angiopoietin-2 causes inflammation in vivo by promoting vascular leakage. *J Pharmacol Exp Ther.* 2005;314(2):738–744.
14. Thurston G, et al. Leakage-resistant blood vessels in mice transgenically overexpressing angiopoietin-1. *Science*. 1999;286(5449):2511–2514.
15. Sundberg C, Kowanetz M, Brown LF, Detmar M, Dvorak HF. Stable expression of angiopoietin-1 and other markers by cultured pericytes: phenotypic similarities to a subpopulation of cells in maturing vessels during later stages of angiogenesis in vivo. *Lab Invest.* 2002;82(4):387–401.
16. Hammes HP, et al. Angiopoietin-2 causes pericyte dropout in the normal retina: evidence for involvement in diabetic retinopathy. *Diabetes*. 2004;53(4):1104–1110.
17. Tidhar A, et al. A novel transgenic marker for migrating limb muscle precursors and for vascular smooth muscle cells. *Dev Dyn.* 2001;220(1):60–73.
18. Feng Y, et al. Impaired pericyte recruitment and abnormal retinal angiogenesis as a result of angiopoietin-2 overexpression. *Thromb Haemost.* 2007;97(1):99–108.
19. Fuxe J, et al. Pericyte requirement for anti-leak action of angiopoietin-1 and vascular remodeling in sustained inflammation. *Am J Pathol.* 2011;178(6):2897–2909.
20. Armulik A, Genove G, Betsholtz C. Pericytes: developmental, physiological, and pathological perspectives, problems, and promises. *Dev Cell.* 2011;21(2):193–215.
21. Kumpers P, et al. Time course of angiopoietin-2 release during experimental human endotoxemia and sepsis. *Crit Care.* 2009;13(3):R64.
22. Witzenbichler B, Westermann D, Knueppel S, Schultheiss HP, Tschope C. Protective role of angiopoietin-1 in endotoxic shock. *Circulation*. 2005;111(1):97–105.
23. David S, et al. Acute administration of recombinant Angiopoietin-1 ameliorates multiple-organ dysfunction syndrome and improves survival in murine sepsis. *Cytokine.* 2011;55(2):251–259.
24. De Domenico I, et al. Hepcidin mediates transcriptional changes that modulate acute cytokine-induced inflammatory responses in mice. *J Clin Invest.* 2010;120(7):2395–2405.
25. Tzepi IM, et al. Angiopoietin-2 enhances survival in experimental sepsis induced by multidrug-resistant Pseudomonas aeruginosa. *J Pharmacol Exp Ther.* 2012;343(2):278–287.
26. Korff T, et al. Angiopoietin-1 mediates inhibition of hypertension-induced release of angiopoietin-2 from endothelial cells. *Cardiovasc Res*. 2012;94(3):510–518.
27. Reiss Y, et al. Angiopoietin-2 impairs revascularization after limb ischemia. *Circ Res.* 2007;101(1):88–96.
28. Dore-Duffy P, et al. Pericyte-mediated vasoconstriction underlies TBI-induced hypoperfusion. *Neurol Res.* 2011;33(2):176–186.
29. Papapetropoulos A, Garcia-Cardena G, Madri JA, Sessa WC. Nitric oxide production contributes to the angiogenic properties of vascular endothelial growth factor in human endothelial cells. *J Clin Invest.* 1997;100(12):3131–3139.
30. Ziche M, et al. Nitric oxide synthase lies downstream from vascular endothelial growth factor-induced but not basic fibroblast growth factor-induced angiogenesis. *J Clin Invest.* 1997; 99(11):2625–2634.
31. Lopez JJ, et al. Hemodynamic effects of intracoronary VEGF delivery: evidence of tachyphylaxis and NO dependence of response. *Am J Physiol.* 1997;273(3 pt 2):H1317–H1323.
32. Sato K, et al. Efficacy of intracoronary or intravenous VEGF165 in a pig model of chronic myocardial ischemia. *J Am Coll Cardiol.* 2001;37(2):616–623.
33. Ahmed A, et al. Angiopoietin-2 Confers atheroprotection in apoE$^{-/-}$ mice by inhibiting ldl oxidation via nitric oxide. *Circ Res*. 2009;104(12):1333–1336.
34. Yu J, et al. Endothelial nitric oxide synthase is critical for ischemic remodeling, mural cell recruitment, and blood flow reserve. *Proc Natl Acad Sci U S A.* 2005;102(31):10999–11004.
35. Lindblom P, et al. Endothelial PDGF-B retention is required for proper investment of pericytes in the microvessel wall. *Gene Dev*. 2003;17(15):1835–1840.
36. Nystrom HC, et al. Platelet-derived growth factor B retention is essential for development of normal structure and function of conduit vessels and capillaries. *Cardiovasc Res*. 2006;71(3):557–565.
37. Schlaeger TM, Qin Y, Fujiwara Y, Magram J, Sato TN. Vascular endothelial cell lineage-specific promoter in transgenic mice. *Development*. 1995;121(4):1089–1098.
38. Deutsch U, et al. Inducible endothelial cell-specific gene expression in transgenic mouse embryos and adult mice. *Exp Cell Res*. 2008;314(6):1202–1216.
39. Yu Z, Redfern CS, Fishman GI. Conditional transgene expression in the heart. *Circ Res.* 1996;79(4):691–697.
40. Horstkotte J, et al. Mitochondrial thioredoxin reductase is essential for early postischemic myocardial protection. *Circulation*. 2011;124(25):2892–2902.
41. Zaruba MM, et al. Synergy between CD26/DPP-IV inhibition and G-CSF improves cardiac function after acute myocardial infarction. *Cell Stem Cell*. 2009;4(4):313–323.
42. Rehberg M, Krombach F, Pohl U, Dietzel S. Label-free 3D visualization of cellular and tissue structures in intact muscle with second and third harmonic generation microscopy. *PLoS One.* 2011;6(11):e28237.
43. Bish LT, et al. AAV9 provides global cardiac gene transfer superior to AAV1, AAV6, AAV7, and AAV8 in the mouse and rat. *Hum Gene Ther.* 2008;19(12):1359–1368.
44. Thomas M, et al. A novel angiopoietin-2 selective fully human antibody with potent anti-tumoral and anti-angiogenic efficacy and superior side effect profile compared to pan-angiopoietin-1/-2 inhibitors. *PLoS One*. 2013;8(2):e54923.